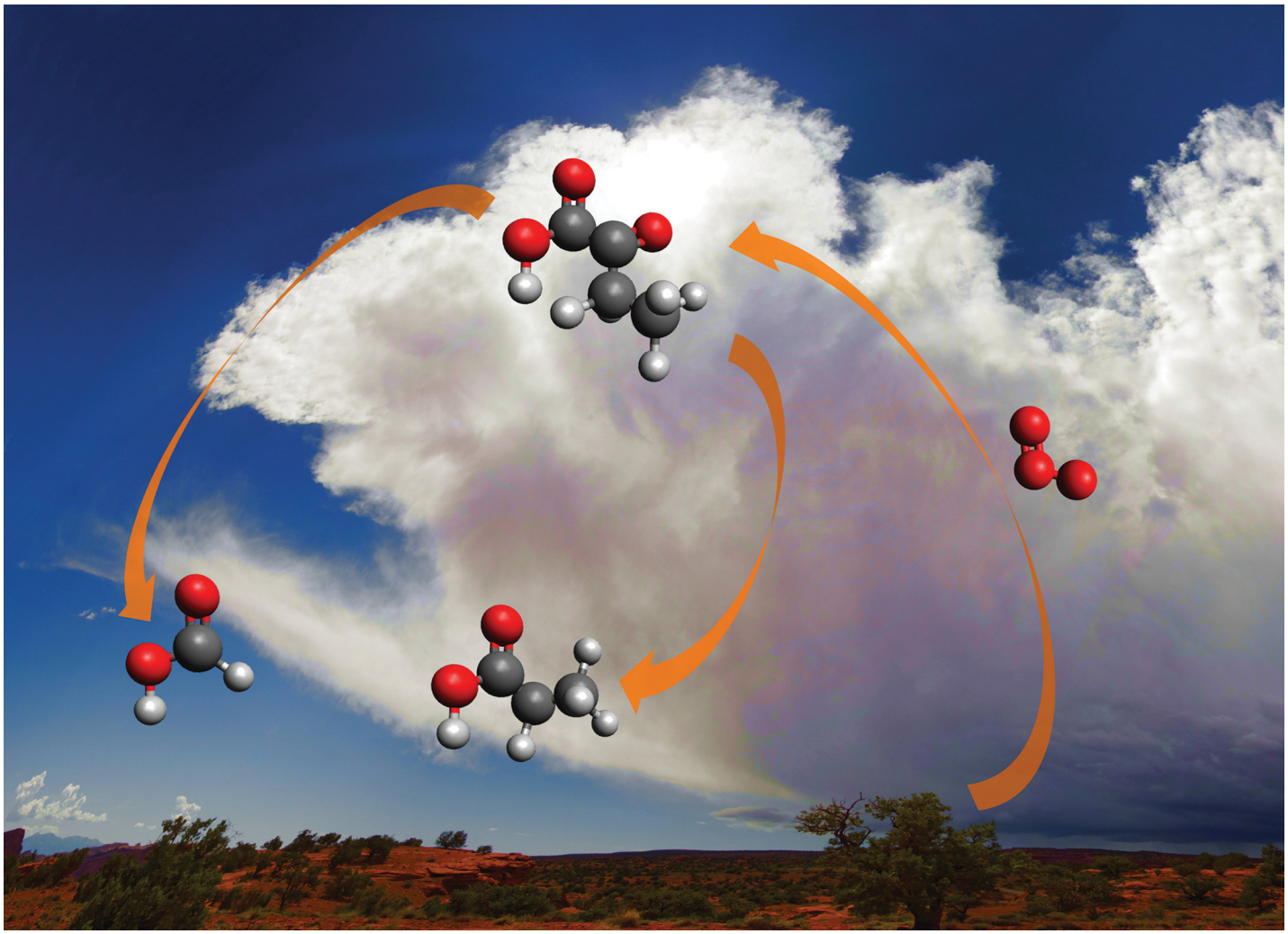

Showcasing research from the Institute for Atmospheric and Environmental Research, University of Wuppertal, Germany.

Organic acid formation in the gas-phase ozonolysis of α,β-unsaturated ketones

The institute comprises research groups dedicated to atmospheric chemistry and physics. The chemistry group covers field measurements by an environmental monitoring station and laboratory studies on heterogeneous and gas-phase chemistry. The institute hosts atmospheric simulation chambers which allow the investigation of gas-phase chemical mechanisms under controlled conditions using a wide range of state-of-the art analytical devices. In this respect, the present chamber studies show the formation of organic acids in the ozonolysis of α,β-unsaturated ketones, confirmable only using complementary experimental approaches.

As featured in:

See Niklas Illmann *et al.*, *Phys. Chem. Chem. Phys.*, 2023, **25**, 106.

ROYAL SOCIETY OF CHEMISTRY

rsc.li/pccp

Registered charity number: 207890

PCCP

ROYAL SOCIETY OF CHEMISTRY

PAPER

View Article Online
View Journal | View Issue

Cite this: *Phys. Chem. Chem. Phys.*, 2023, **25**, 106

Organic acid formation in the gas-phase ozonolysis of α,β-unsaturated ketones†

Niklas Illmann, * Iulia Patroescu-Klotz and Peter Wiesen

Organic acids are key species in determining the radiative properties of the atmosphere due to their contribution to particle formation. Reported discrepancies between field measurements and modelling suggest significant missing sources. Herein, we present a mechanistic investigation on the gas-phase ozonolysis of ethyl vinyl ketone (EVK, 1-penten-3-one), which we chose as a model compound for α,β-unsaturated ketones. Experiments were performed in a 1080 L quartz-glass reaction chamber (QUAREC) at 990 ± 15 mbar and 298 ± 2 K (r. h. ≪ 0.1%) and analysed *via* long-path FTIR spectrometry and PTR-ToF-MS. The experiments were performed in the presence of an excess of CO to suppress the chemistry of OH radicals. For a comprehensive picture, in selected experiments, SO_2 was also added to the reaction system to scavenge the stabilized Criegee intermediates (sCIs) and to investigate their formation yield. Combining the results of both set-ups allowed us to quantify 2-oxobutanal, for which we report vapour-phase FTIR spectra. In addition, we introduce the first-ever infrared spectra of perpropionic acid, which was also positively identified in the EVK + O_3 system. A detailed analysis of the experimental findings allowed us to link the identified reaction products (acetaldehyde, ethyl hydroperoxide, and perpropionic acid) to known bimolecular reactions of RO_2 radicals. Thereby, it is shown that the EVK + O_3 reaction yields formic acid, HC(O)OH, and propionic acid, $C_2H_5C(O)OH$, and their formation is not covered by mechanisms reported in the literature. Three different pathways accounting for their formation from chemically activated CIs are proposed and possible implications for the ozonolysis of α,β-unsaturated ketones in the atmosphere are discussed.

Received 13th July 2022,
Accepted 11th November 2022

DOI: 10.1039/d2cp03210d

rsc.li/pccp

Introduction

Organic acids are a class of atmospheric compounds that, with the exception of formic acid, HC(O)OH, and acetic acid, $CH_3C(O)OH$, determined also in the gas-phase, are mainly found in aerosol particles, which explains their importance for rainwater pH, cloud growth and chemistry and hence the radiative properties of the atmosphere.[1–3]

However, a series of studies have shown significant discrepancies between model predictions concerning their chemical formation and ground-based and airborne observations.[4–6] For example, models under-predict formic acid concentrations by up to a factor of 10,[5,6] indicating a large gap in our understanding of carboxylic acid forming mechanisms. Several investigations revealed candidates for the missing sources. These contained the OH chemistry of isoprene oxidation products including isoprene nitrates[7] or α-hydroxy carbonyls like glycolaldehyde[8] and hydroxyacetone,[9] the OH oxidation of enols[10] or reactions of Criegee intermediates (mainly CH_2OO) with water vapour.[11,12] Yet, even when these "candidate sources" were included in models, HC(O)OH remains underestimated by up to a factor of 3.[5] Recently, the formation of ketene-enols in the OH oxidation of aromatic species and their further reactions with OH and O_3 were suggested to account for the rapid photochemical formation of organic acids in urban areas.[13] However, modelling studies revealed also that the interplay of different sources is needed to account for the missing levels of small organic acids, many of them associated though with isoprene chemistry or the oxidation of biogenic volatile organic compounds (BVOCs) in general.[5]

Ozonolysis reactions were considered mainly as a source of larger carboxylic acids (derived from larger alkenes and terpenes), easily partitioning into the aerosol phase. In many cases, the overall mechanism and the reaction products of ozonolysis reactions remain poorly characterized, which is often reflected by a low overall carbon balance. This is partly due to the nature of ozonolysis reactions, which proceed almost exclusively (with some exceptions, *e.g.* epoxide formation) *via* a 1,3-dipolar cycloaddition yielding initially a five-membered primary ozonide (POZ). This, in turn, is formed loaded with a

Institute for Atmospheric and Environmental Research, Bergische Universität Wuppertal, Gaußstraße 20, 42119 Wuppertal, Germany.
E-mail: illmann@uni-wuppertal.de

† Electronic supplementary information (ESI) available. See DOI: https://doi.org/10.1039/d2cp03210d

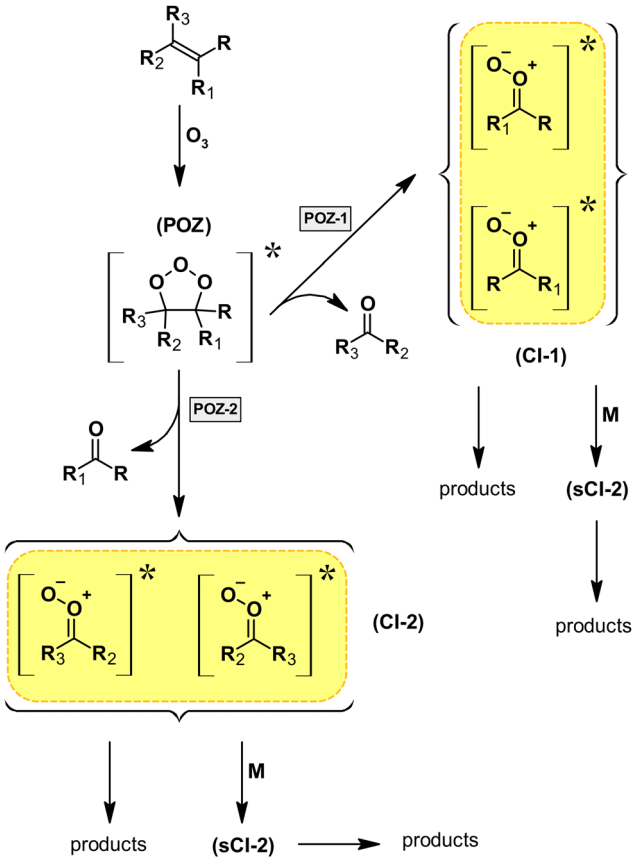

Fig. 1 Generalized mechanism for the gas-phase ozonolysis of unsaturated organic species proceeding through the initially formed primary ozonide (POZ) and subsequent possible decomposition pathways (POZ-1 and POZ-2), yielding a stable carbonyl species and a Criegee intermediate (CI). Two stereoisomers are possibly formed for each CI, which results in four possible CIs in total.

substantial amount of energy due to the exothermicity of ozonolysis reactions. As a consequence, the POZ will decompose immediately following two possible pathways (see Fig. 1), where only 50% results initially in the formation of stable carbonyl products (primary carbonyls), if the POZ channel represents the only pathway of the ozonolysis reaction. The remaining fraction yields Criegee intermediates (CIs), which are described formally as zwitterionic carbonyl oxides (see Fig. 1). Since the excess energy is necessarily distributed among the initially formed reaction products, this results in nascent CIs, which are subject to further decomposition, whereas a fraction might be thermalized (stabilized CIs = sCIs) and is prone to bimolecular reactions.[14] Extensive work during the last few decades has shown that sCIs react very fast with SO_2 and organic acids (*e.g.* ref. 14 and references therein), although under atmospheric conditions, sCIs will react preferentially with H_2O or the water dimer. This suggests that the different levels of H_2O present in the experimental systems might be one reason for the difference in the product distributions reported by various authors. Furthermore, ozonolysis reactions are also experimentally challenging, as they were shown to produce OH radicals (*e.g.* ref. 14 and references therein), which infer a competition between the O_3 and OH reactions of the target species. In order to overcome this issue, OH scavengers like cyclohexane or CO are often used to investigate the ozonolysis system without OH interference in atmospheric simulation chamber experiments. However, in the case of CO, almost any OH radical is converted into HO_2, which might imply a significant increase of the HO_2 level in the reaction system.

$$CO + OH + O_2 \rightarrow CO_2 + HO_2 \quad (R1)$$

By contrast, the OH-initiated oxidation of cyclohexane forms additional RO_2 species, *e.g.* initially the cyclohexyl peroxy radical.

$$c\text{-}C_6H_{12} + OH + M\ (+O_2) \rightarrow c\text{-}C_6H_{11}O_2 + H_2O + M^* \quad (R2)$$

Since at higher O_3 levels, any background level of NO present in a simulation chamber is ultimately titrated,

$$NO + O_3 \rightarrow NO_2 + O_2 \quad (R3)$$

the further fate of the RO_2 radicals is (besides possible isomerization if the HO_2 or RO_2 levels were sufficiently low in the experiment) dominated by reactions with either HO_2 or RO_2.

$$RO_2 + HO_2 \rightarrow \text{products} \quad (R4)$$

$$RO_2 + RO_2 \rightarrow \text{products} \quad (R5)$$

Hence, the used OH scavenger might affect the observed product distribution *via* reactions (R4) and (R5).

It was shown that α,β-unsaturated ketones are formed in the oxidation of BVOCs (*e.g.* methyl vinyl ketone from isoprene) or are directly released by vegetation under stress conditions (*e.g.* ethyl vinyl ketone was reportedly emitted upon leave wounding[15]). Despite the importance of α,β-unsaturated ketones in terms of their atmospheric burden, their ozonolysis reactions were scarcely studied. Furthermore, the existing studies report rather contradictory results, for example, in the case of the primary carbonyls obtained from methyl vinyl ketone + O_3.[16,17] For the longer-chain analogue ethyl vinyl ketone (EVK, 1-penten-3-one), only two studies were reported previously by Grosjean *et al.*[16] and O'Dwyer *et al.*,[18] both targeting the primary carbonyl formation. Grosjean *et al.*[16] identified also acetaldehyde, although its formation remained unexplained. Current recommendations by the IUPAC (International Union of Pure and Applied Chemistry) Task Group on Atmospheric Chemical Kinetic Data Evaluation are limited to small alkenes and terpene-derived CIs.[14] Combining this, the fate of carbonyl-substituted CIs, where the C=O bond is close to the $C{=}O^+{-}O^-$ moiety, seems to be generally poorly understood. Considering the available kinetic data for the OH and O_3 reaction of MVK[19] (see ref. 20 for a list of available literature data on the MVK + O_3 rate coefficient) and EVK,[21,22] the ozonolysis reactions account for about 17% of the MVK and about 15% of the EVK daytime loss, respectively (for [OH] ≈ 1×10^6 cm^{-3} and [O_3] ≈ 35 ppbV). In an attempt to close the existing gaps in the α,β-unsaturated ketone ozonolysis mechanism, we studied in the present work the reaction of ozone with EVK, chosen as a model species for the title compounds.

To keep the reaction system as simple as possible, two experimental approaches were followed. First, all experiments were performed with an excess of CO to suppress OH reactions and exclude the formation of RO_2 radicals other than formed from EVK + O_3. In a second series of experiments, sufficient SO_2 was also added to the reaction mixture to favour the sCI + SO_2 reaction and hence suppress potential reactions of sCIs with other reaction products. Combining the results of both experimental set-ups provided a more comprehensive perspective on the ozonolysis mechanism. Clear evidence was found for the formation of organic acids and pathways accounting for their formation are proposed. In pursuing this issue, we were able to obtain the infrared absorption features of gaseous perpropionic acid.

Experimental

In order to investigate the EVK + O_3 system, experiments were carried out in a 1080 L quartz reaction chamber (QUAREC) under dry conditions (r.h. $\ll$ 0.1%) at 990 $\pm$ 15 mbar of synthetic air and a temperature of 298 $\pm$ 2 K. The chamber is coupled to a Fourier-transform infrared (FTIR) spectrometer (Nicolet iS 50) by means of a White-type mirror system. FTIR spectra were recorded in the spectral range of 4000–700 cm^{-1} at a resolution of 1 cm^{-1}. The system is operated at an optical path length of 484.7 $\pm$ 0.8 m. The current set-up of the QUAREC chamber is described in greater details elsewhere.[23]

The initial mixing ratios were 1.5–2.3 ppmV for EVK (Alfa Aesar, 97%), 3.1–4.0 ppmV for SO_2 (Air Liquide, 99.9%), and 15 000–20 000 ppmV for CO (Air Liquide, 99.97%), where 1 ppmV = 2.46 $\times$ 10^{13} cm^{-3} (at 298 K and 1 atm).

EVK and the reaction products were quantified *via* FTIR spectroscopy using calibrated reference spectra from the internal laboratory database. A list of the used integrated absorption cross sections is given in the ESI† (Table S1). In the experiments, typically 50–70 interferograms were co-added per spectrum, which results in averaging recording periods of about 80–115 s. In addition to the quantification by long-path FTIR spectroscopy, a qualitative identification of reaction products was performed using a PTR-ToF-MS 8000 instrument (Ionicon Analytik GmbH, Innsbruck, Austria) in experiments without SO_2 injection. The drift tube was operated at a temperature of 70 °C, 2.2 mbar pressure and 500 V drift voltage. Accordingly, the E/N value was about 120 Td (1 Td = 1 $\times$ 10^{-17} V cm^2), where E is the electric field in the drift tube, and N is the gas number density. The sampling line of the instrument was operated at a temperature of 70 °C and coupled to a heated stainless steel line, which was mounted on the middle flange of the 1080 L chamber. The sample flow was 200 mL min^{-1}. In order to obtain stable signals with the PTR-MS instrument, the fan mounted on the middle flange inside the chamber was switched on during the whole experiment. The PTR-ToF-MS data were recorded and processed using the TOFDAQ data acquisition software and the PTR-MS VIEWER software (Ionicon Analytik GmbH, Innsbruck, Austria), respectively.

The reaction mixtures were observed over a period of 15–50 min without an oxidant in order to determine the wall loss in each individual experiment. After that, the reaction was started by the injection of O_3, which was generated by passing a stream of pure oxygen (Messer, 99.995%) through an electrical discharge in a homemade device. Typically, the formation of reaction products was observed over a period of about 20 min.

Simulations of the temporal evolution of reaction products, possibly formed from peroxy radical reactions, were performed following the approach outlined previously.[23] A detailed description of the sensitivity analysis and model validation can be found elsewhere.[24] In contrast to previous applications, an explicit chemical mechanism was used for the relevant RO_2 reactions, in order to prove if the temporal behaviour of selected reaction products can be described by known reaction sequences. For this purpose, the source of the parent RO_2 was included in a simplified reaction (EVK + O_3 $\rightarrow$ x_1RO_2 + $x_2R'O_2$) as well as an average HO_2 concentration. Both the branching ratio towards the RO_2 formation and [HO_2] were varied to check for a match between the experimental data and the modelled time profiles for all relevant species.

Results and discussion

The wall loss of EVK was found to be in the range (1–5) $\times$ 10^{-5} s^{-1}. The loss due to the O_3 reaction was about (6–8) $\times$ 10^{-4} s^{-1} and hence at least one order of magnitude faster than the wall loss in all performed experiments. The EVK + O_3 reaction was observed until about 50–80% of the EVK was consumed. Table 1 summarizes the yields of the quantified reaction products based on the FTIR measurements together with the assigned ion signals from the PTR-MS data. A detailed discussion on the assignment of ion signals is presented in Section B of the ESI.†

a. EVK + O_3 in the presence of SO_2

The FTIR spectra show unambiguously the formation of formaldehyde (HCHO), HC(O)OH, propionic acid, acetaldehyde and carbon dioxide (CO_2). In all cases, the yield plots are highly linear in the initial stages of the ozonolysis reaction, where the product formation is large, suggesting their formation as first-generation closed-shell products. For HC(O)OH, a non-linear behaviour is observed at long reaction times (Fig. 2), which is likely the result of a significant wall loss at higher HC(O)OH concentrations. The reported errors (Table 1) are a combination of the 2σ statistical error and the overall accuracy of the measurements. Due to the usage of carbon monoxide, CO, as an OH radical scavenger, the reported CO_2 yield consists of CO_2 formed from both the ozonolysis reaction and from the reaction of CO with OH radicals.

Up to 20% of SO_2 initially added is consumed during the EVK + O_3 reaction. A plot of the consumed SO_2 *vs.* the consumed EVK (Fig. S1, ESI†) yields a slope of 0.40 $\pm$ 0.09, where the error represents the overall accuracy as mentioned above. The results of different experimental runs were reproducible within 4%. Since only the overtone of SO_2 in the range 2530–2440 cm^{-1} could be used for the evaluation of the FTIR spectra, we prefer to assign an expanded uncertainty of 20%.

Table 1 Quantified reaction products and assigned masses of the EVK + O_3 reaction in the presence of CO as an OH radical scavenger and a supplementary addition of SO_2 together with available literature data. The uncertainties given for the product yields determined within this work represent a combination of the 2σ statistical error and the accuracy error

Species	Yield[a]	Yield[b]	Yield[a]	Yield[c]	Assigned m/z[a]
HCHO	0.28 ± 0.10	0.548 ± 0.069	0.37 ± 0.02	0.65 ± 0.12	31.018 (CH_3O^+)
2-Oxobutanal	0.29 ± 0.10[d]	0.444 ± 0.025	0.49 ± 0.03	0.53 ± 0.12[d]	87.045 ($C_4H_7O_2^+$), 59.050 ($C_3H_7O^+$)
Formic acid	0.012 ± 0.008			0.12 ± 0.06	47.013 ($CH_3O_2^+$)
Formic anhydride	0.14 ± 0.08				47.013 ($CH_3O_2^+$)
Formic propionic anhydride	0.11 ± 0.04				75.045 ($C_3H_7O_2^+$), 47.013 ($CH_3O_2^+$)
Acetaldehyde	0.10 ± 0.04	0.097 ± 0.001		0.15 ± 0.05	45.034 ($C_2H_5O^+$)
Ethyl hydroperoxide	0.14 ± 0.05				45.034 ($C_2H_5O^+$)
Perpropionic acid	0.065 ± 0.043			n.q.	91.040 ($C_3H_7O_3^+$), 75.045 ($C_3H_7O_2^+$)
Propionic acid				0.17 ± 0.03	
Propionaldehyde[e]					59.050 ($C_3H_7O^+$)
Methyl ketene[e]					57.034 ($C_3H_5O^+$)
CO_2[f]	0.90 ± 0.21			0.54 ± 0.08	
sCI				0.40 ± 0.09	
Detection method	FTIR	LC-UV	FTIR	FTIR	PTR-MS
Ref.	This work	Grosjean *et al.*[16]	O'Dwyer *et al.*[18]	This work	This work

[a] Experiments were performed in the presence of CO as an OH radical scavenger. [b] Experiments were performed in the presence of cyclohexane as an OH radical scavenger. [c] Experiments were performed in the presence of CO as an OH radical scavenger and SO_2. [d] The yields were obtained following a semi-quantitative approach by assuming the infrared cross section of the C=O band to equal the cross section of the structural analogue methyl glyoxal. [e] The formation is not unequivocally proven due to interfering fragment ions. [f] Sum of CO_2 formed from the reaction of EVK + O_3 and CO + OH.

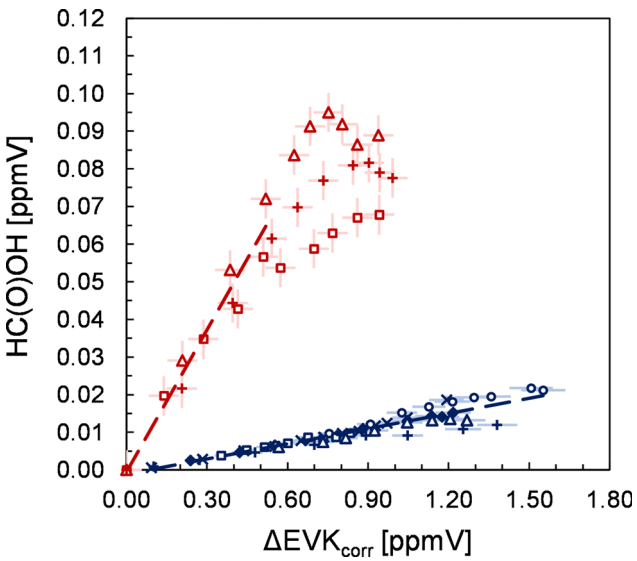

Fig. 2 Yield plots obtained for formic acid in the presence (red) and absence (blue) of SO_2. Different experimental runs are denoted using different symbols. The error bars represent a precision error as a combination of a relative error plus the corresponding detection limit under the experimental conditions.

The decomposition of the primary ozonide (POZ), which is formed through the 1,3-dipolar cycloaddition according to the well-established ozonolysis mechanism,[25] is expected to proceed *via* two pathways, forming either HCHO and a carbonyl-substituted Criegee intermediate (CI) or 2-oxobutanal and formaldehyde oxide, CH_2OO. The consumption of SO_2 during the ozonolysis reaction indicates the formation of stabilized CIs in the reaction system. Since the CH_2OO + SO_2 reaction results mainly in the production of formaldehyde,[26] the HCHO yield observed in the presence of SO_2 represents the sum of the primary HCHO and the bimolecularly formed HCHO.

Theoretical calculations by Vereecken *et al.*[27] suggest that for a large fraction of stabilized CIs, unimolecular loss might be still faster than bimolecular reactions. Based on the SAR approach presented in the same publication,[27] the rate coefficients for the unimolecular loss (1,3-cyclisation) are calculated to be 0.3 s^{-1} (CH_2OO), 0.04 s^{-1} (*E*-$C_2H_5C(O)CHOO$), and 20 s^{-1} (*Z*-$C_2H_5C(O)$-CHOO) for the sCIs possible in the present reaction system. Since rate coefficients for the sCI + SO_2 reaction are expected to be in the range 10^{-11}–10^{-10} cm^3 s^{-1},[27] it is likely that unimolecular loss is not competitive with the SO_2 reaction under the present experimental conditions. In addition, the linearity of the plots (Fig. S1, ESI†) over the whole experimental duration suggests that the level of SO_2 was sufficiently high to suppress the reaction of sCIs with the acids formed in the reaction system. Nevertheless, we prefer the sCI yield obtained here to be regarded as a lower limit.

Trace (a) in Fig. 3 shows a residual FTIR spectrum of an experiment after the subtraction of all undoubtedly identified species mentioned above. In all experiments with added SO_2, a non-linear baseline shift is observed, which strongly indicates the formation of particles in the experimental system. This can be rationalized through the size-dependent scattering of IR radiation when particle diameters are similar to the wavenumber of the radiation and the particle concentration is sufficiently high. The particle-based scattering lowers the IR radiation intensity entering the detector of the spectrometer. Hence, a broad absorption becomes visible in the FTIR spectra. Given that this effect is not observed in the absence of SO_2, this is interpreted as the formation of H_2SO_4 due to the reaction of SO_3, formed from the reaction of SO_2 with sCIs, with a trace amount of H_2O present in the reaction system.

Trace (b) shows the same residual spectrum after applying a baseline correction. Since all other identified reaction products

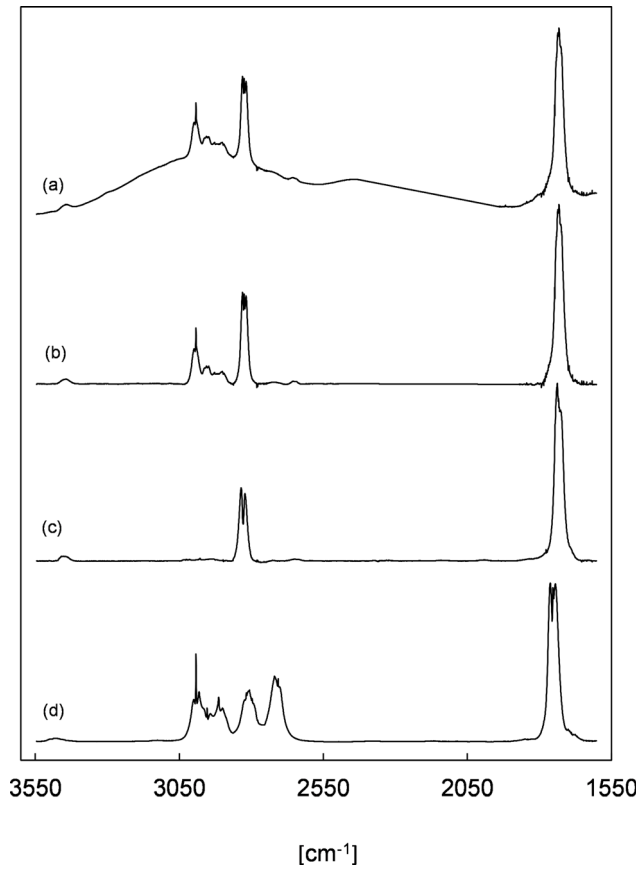

Fig. 3 (a) Residual spectrum assigned to 2-oxobutanal (ethyl glyoxal) from an EVK + O_3 experiment in the presence of CO used as an OH radical scavenger and SO_2 used as a sCI scavenger (the spectrum was cut in the range of 2400–1900 cm^{-1}), (b) spectrum (a) after baseline correction, (c) reference spectrum of methyl glyoxal, and (d) reference spectrum of propionaldehyde.

were subtracted at this point and secondary reactions were largely minimized due to the addition of SO_2, the residual absorption bands visible in the range of 3500–1600 cm^{-1} should correspond mainly to 2-oxobutanal. For comparison, trace (c) shows a reference spectrum of gas-phase methyl glyoxal, which possesses characteristic absorption features for the C═O stretching vibrations centred at 1730 cm^{-1} and for the C–H stretching vibration of the aldehyde moiety in the range 2860–2800 cm^{-1}. Both position and relative intensity of these absorption bands are similarly found in the residual spectrum in panel (b). Additionally, the absorption pattern around 3000 cm^{-1} (C–H stretching vibration of alkyl groups) is quite similar to the gas-phase FTIR spectrum of propionaldehyde presented in panel (d). This all supports the assignment of the residual spectrum to 2-oxobutanal.

Taking into account that absorption cross sections of characteristic vibrations usually do not show a large variability for structurally similar compounds, a quantitative FTIR spectrum of 2-oxobutanal was obtained by applying the infrared cross section of the methyl glyoxal C═O absorption band[28] to the baseline-corrected residual spectrum, which allowed to calculate the dicarbonyl yield as listed in Table 1.

b. EVK + O_3 in the absence of SO_2

In the absence of SO_2, the FTIR spectra show the formation of HCHO, 2-oxobutanal, HC(O)OH, formic anhydride (FA), formic propionic anhydride (FPA), acetaldehyde, ethyl hydroperoxide and CO_2. Through separate experiments, in which we irradiated propionaldehyde/methanol/Cl_2 mixtures, we obtained reference spectra of gas-phase perpropionic acid (Fig. 4, see the ESI† for details). The characteristic absorption band of the O–H stretching vibration centred on about 3303 cm^{-1} allowed us to identify the peracid as a reaction product of the EVK + O_3 reaction. Applying available cross sections for peracetic acid[29] provides an estimate of the perpropionic acid yield as listed in Table 1. Due to this semi-quantitative approach, an expanded uncertainty of 50% was added to the statistical error.

The formation of all organic species is further supported by the presence of characteristic signals in the PTR mass spectra (see the ESI,† for details). The yield plot of FA, combining the FTIR data of all experimental runs, is shown in panel (a) of Fig. 5. In each experiment, the correlation is linear, but different slopes are observed, which is reflected in the large error assigned to the FA yield. In fact, when considering all experimental data, the plot suggests a larger FA yield at higher EVK consumption levels, hence at long reaction times.

As presented in panel (b) of Fig. 5, the FPA data of each single experiment do not exhibit significant scatter, indicating a small precision error in the FPA quantification *via* the FTIR spectra. The profiles of all experimental runs evidence a non-linear behaviour suggesting also an increase in the FPA yield with longer reaction times. It appears that although the profiles are precisely non-linear, significant differences are found for correlations of different experimental runs.

However, when the FPA yields are determined from the data at higher EVK consumption levels, they are found to be reproducible within a factor of 1.2 with the exception of one experiment. This argues against systematic errors in the FPA quantification in different experimental runs. Thus, it appears that on the one hand, both anhydrides are formed delayed (although this is less obvious in the case of FA) and hence do

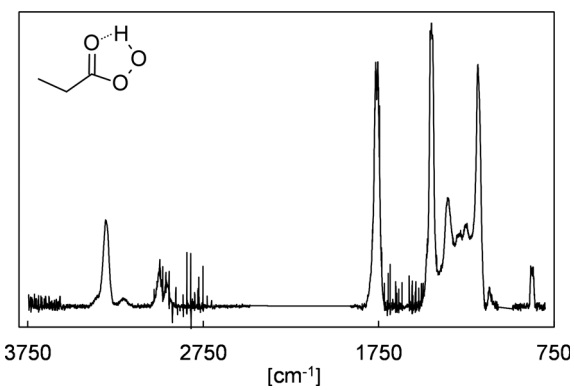

Fig. 4 Gas-phase infrared spectrum assigned to perpropionic acid (peroxypropionic acid), $CH_3CH_2C(O)OOH$, obtained from irradiating a propionaldehyde/methanol/Cl_2-mixture. The spectrum was baseline-corrected and cut in the range of 2400–1900 cm^{-1} and 1070–990 cm^{-1}.

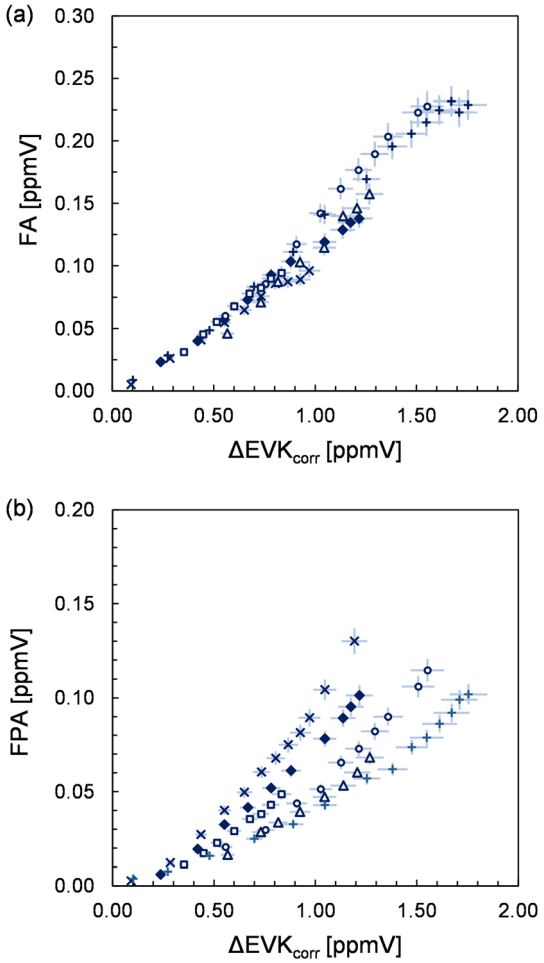

Fig. 5 Yield plots obtained for (a) formic anhydride (FA) and (b) formic propionic anhydride (FPA). Different experimental runs are denoted using different symbols. The error bars represent a precision error as a combination of a relative error plus the corresponding detection limit under the experimental conditions.

not result directly from the CI further reactions. On the other hand, the delay seems to differ from one to the other experiment in the case of formic propionic anhydride.

FA cannot result directly from the ozonolysis reaction itself, which is indicated by the yield plot (Fig. 5) as discussed above. Its formation is expected to proceed through the bimolecular reaction of formaldehyde oxide with formic acid resulting in the generation of hydroperoxymethyl formate (HPMF), as observed in previous studies.[30,31] The spectral features observed here do not support the existence of HPMF. However, it was reported that HPMF decomposition leads to H_2O and formic anhydride,[30,31] which is, therefore, indirect evidence for HC(O)OH formation in the system. Nearly all formic acid is consumed *via* the fast reaction of HC(O)OH + sCI. This is confirmed, on the one hand, by the large increase of the HCHO yield in the presence of SO_2, indicating a large fraction of thermally equilibrated formaldehyde oxide prone to bimolecular reactions. On the other hand, the consumption of HC(O)OH through sCIs is being suppressed in the presence of SO_2, which leads to the observed substantial increase in the HC(O)OH yield. Since both formic acid and HPMF influence the formation of FA, the FA yield is highly sensitive to the further fate of both precursor species. This supposedly explains the variation observed for the FA yield (Fig. 5). For instance, if HC(O)OH exhibits a significantly larger wall loss in one experiment, this will result necessarily in a lowering of HPMF and consequently in a lower FA yield. This appears to be even more important in the case of FPA. Since the yield plots do unambiguously suggest its formation from secondary reactions, we can only imagine a reaction sequence in analogy to HC(O)OH + CH_2OO to explain the formation of the mixed anhydride. Accordingly, FPA is expected to result from the decomposition of hydroperoxymethyl propionate (HPMP) formed following a reaction of propionic acid with CH_2OO. Overall, the formation of both anhydrides and the shape of their yield plots evidence the formation of HC(O)OH and propionic acid in the EVK + O_3 reaction.

c. Comparison

The primary carbonyl yields observed in the absence of SO_2 suggest a 1 : 1 ratio for the POZ decomposition channels. However, this would imply that in the present investigation, the POZ decomposition accounts solely for about 57 ± 14% of the EVK + O_3 reaction. The experimental results do not provide any hint for other reactions, *e.g.* the formation of an epoxide. At the same time, the increase of the HCHO + 2-oxobutanal yield employing large SO_2 concentrations is significantly larger than can be explained by sCI + SO_2 reactions. We do not find any conclusive explanation for this behaviour (the error analysis is provided in Section E of the ESI†) and can only speculate that an unidentified secondary consumption of the primary carbonyls exists in the experimental system in the absence of any sCI scavenger.

The gas-phase ozonolysis of EVK has been formerly investigated by Grosjean *et al.*[16] and O'Dwyer *et al.*[18] Grosjean and co-workers[16] reported product yields of 0.548 ± 0.069 and 0.444 ± 0.025 for HCHO and 2-oxobutanal, respectively. The quantification of the carbonyls was done by liquid chromatography, after the collection of samples onto DNPH-coated cartridges.[16] Both the HCHO and 2-oxobutanal yields we determined are significantly lower than those reported by Grosjean *et al.*[16] In contrast to the present work, the former study has been carried out at a relative humidity of 55 ± 10%. Although the bimolecular reaction of formaldehyde oxide with H_2O is quite slow[14] ($\approx 10^{-16}$ cm^3 s^{-1}), at least a fraction of the stabilized CH_2OO will react with H_2O under these experimental conditions. The CH_2OO + H_2O as well as the CH_2OO + $(H_2O)_2$ reactions have been shown to form initially the chemically activated hydroxymethyl hydroperoxide, $OHCH_2OOH$,[32] which is either thermalized or decomposes into HC(O)OH and H_2O or HCHO and H_2O_2. Therefore, an additional source of HCHO might have been present under the humid conditions of the former study. However, since at least for the reaction with the water dimer, other studies provided contradictory conclusions on the relative importance of each reaction channel,[12,14,33] no clear statement can be made. On the other hand, no data are

available for the carbonyl-substituted CI. Due to the lack of a standard, Grosjean *et al.*[16] used a response factor estimated from the results of other α-dicarbonyls, where standards were available, for the quantification of 2-oxobutanal. Accordingly, they assigned a 20% relative error to the 2-oxobutanal response factor. Therefore, the relative error of <6% reported for the 2-oxobutanal yield under humid conditions[16] is at least surprisingly low.

By contrast, O'Dwyer *et al.*[18] worked at a relative humidity <1%. They reported product yields of 0.37 ± 0.02 and 0.49 ± 0.03 for HCHO and 2-oxobutanal, respectively. The present value for HCHO is, thus, within the assigned uncertainty, identical to that of O'Dwyer *et al.*[18] Similar to the present approach, O'Dwyer and co-workers[18] quantified 2-oxobutanal by assuming the cross section of C=O absorption to be the same as for a structurally similar compound, namely *n*-butanal. Following this rationale, they obtained a 2-oxobutanal yield which is about 60% larger than that determined here. Comparing the cross section of the integrated carbonyl absorption band of methyl glyoxal (*e.g.* Talukdar *et al.*[28]) with a value for the C=O absorption band of *n*-butanal from the Wuppertal laboratory database, it is found that the cross section is about ≈65% larger in the case of the α-dicarbonyl. Consequently, the experimentally observed correlation between the integrated carbonyl absorption of 2-oxobutanal and the consumption of EVK is nearly the same in the present study and that of O'Dwyer *et al.*[18] The authors argue solely that the cross section of *n*-butanal was chosen due to the similarities between the residual spectrum and that of *n*-butanal. By contrast, they do not state why they expect the intensity of the C=O absorption of an α-dicarbonyl to be the same as for an aldehyde containing only one carbonyl group, which is intriguing.

d. Mechanistic interpretation

The formation of perpropionic acid and ethyl hydroperoxide can solely be rationalized through the reaction of their parent RO_2 radical with HO_2. Accordingly, the level of HO_2 in the system must be sufficiently high to allow a competition between $RO_2 + HO_2$ and $RO_2 + RO_2$ reactions. This is likely the result of OH radicals formed from the EVK + O_3 reaction, which in the presence of an excess of CO are converted nearly quantitatively into HO_2 radicals, or the result of H atoms following CI fragmentation.

At the same time, the hydroperoxides evidence the formation of both propionyl peroxy, $C_2H_5C(O)O_2$, and ethyl peroxy radicals, $C_2H_5O_2$. Following available literature data,[34–37] the presence of $C_2H_5C(O)O_2$, $C_2H_5O_2$ and HO_2 suggests the RO_2 reaction sequence to evolve in the reaction system as presented in Fig. 6. This in turn accounts for the acetaldehyde formation through RO_2 permutation reactions of the ethyl peroxy radical.[35] The acetaldehyde yield observed in the absence of SO_2 is in good agreement with the value reported by Grosjean *et al.*[16] Since RO_2 reactions were not considered in the former study, the authors did not provide a conclusive explanation for acetaldehyde formation.

In the presence of SO_2, a small curvature around 3300 cm^{-1} might indicate the formation of perpropionic acid. However, a reliable quantification is not possible due to the baseline shift during the reaction, as discussed above. At the same time, no ethyl hydroperoxide was observed, whereas the acetaldehyde yield increased. This suggests both the RO_2 and HO_2 levels to be lower when the sCI scavenger is present, which would imply that the RO_2 species result partly from sCI.

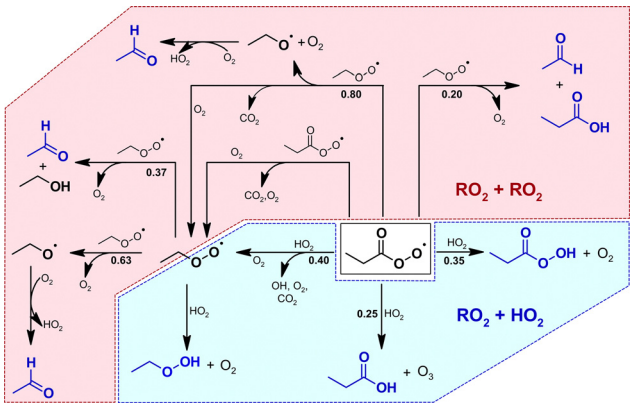

Fig. 6 Chemistry of the propionyl peroxy and ethyl peroxy radical based on the identified reaction products (blue structures). For clarity, the reaction sequences are only shown considering a prompt propionyl peroxy radical source in the experimental system. The blue area represents the $RO_2 + HO_2$ reactions, the rose area marks the $RO_2 + RO_2$ domain. The corresponding branching ratios, given in bold numbers, are the current IUPAC recommendations (2021). For the $C_2H_5C(O)O_2 + HO_2$ reaction, the values are taken from Hasson *et al.*[37]

Simulations on the experiments without SO_2 addition were performed considering the reaction sequence shown in Fig. 6. Since ethyl peroxy radicals might result solely from $C_2H_5C(O)O_2$ further reactions or as well from CI decomposition, we simulated both scenarios for all experiments. The details of this analysis are presented in Section D of the ESI† and only the main conclusions are briefly summarized here.

The temporal evolution of acetaldehyde, ethyl hydroperoxide and perpropionic acid can be reproduced using experimentally plausible HO_2 concentrations (2.3×10^{10} cm^{-3} on average). Accordingly, there is no reason to argue against their time profiles being properly described by the peroxy radical reaction sequence presented in Fig. 6, *e.g.* an additional source of acetaldehyde. At the same time, it is not possible to conclude whether the ethyl peroxy radical evolves solely from the propionyl peroxy radical further chemistry or also promptly from the CI chemistry. For the latter case, all model runs suggest the $C_2H_5O_2$ source to be a factor of ≈5 smaller than the $C_2H_5C(O)O_2$ source with an overall RO_2 radical yield below 40%.

The simulations predict an upper limit of 7% for the propionic acid yield in the absence of SO_2. The acid appears to be entirely consumed *via* the reaction with stabilized CH_2OO, as discussed above, which finally converts propionic acid into FPA. However, considering the FPA yield of 0.11 ± 0.04 at the end of the experiments, this indicates an additional source of propionic acid. In the presence of SO_2, we find a reproducible propionic acid/acetaldehyde ratio of 1.1 ± 0.2, which is more than a factor of 2 larger than possible from the RO_2 reaction

sequence (see Section D of the ESI† for further analysis). Apparently, there is an additional source for propionic acid in the EVK ozonolysis mechanism besides the RO_2-based formation route. In addition, since propionic acid is observed under conditions, where sCI reactions are drastically minimized, this suggests strongly its formation from chemically activated carbonyl oxides.

The formation of stabilized acids was reported for larger CIs following the 1,3-ring closure and subsequent isomerization according to the dioxirane route.[38–40] This may be interpreted in terms of a larger probability of collisional stabilization due to a larger number of vibrational modes comparative to smaller CIs, which potentially allows the excess energy to be distributed below a dissociation threshold. However, since the POZ decomposition yields initially a C_1- and a C_4-fragment, the above mentioned mechanism cannot account for the formation of C_3-acid (propionic acid). This, in turn, would result into 2-oxobutanoic acid, for which no evidence is observed in the PTR mass spectra, nor in the FTIR spectra, assuming a similar spectral structure as the infrared spectra of gas-phase pyruvic acid (2-oxopropanoic acid).

Nevertheless, the prompt formation of the $C_2H_5C(O)O_2$ radical (and possibly of the $C_2H_5O_2$ radical) and the amount of propionic acid, not accounted for by RO_2 further reactions, can only originate from the C_4-fragment, namely the carbonyl-substituted CI. The carbonyl group in α-position prohibits the possibility of an 1,4-H shift isomerization and the intermediate formation of a vinyl hydroperoxide. Therefore, this CI is expected to undergo mainly an isomerization following a 1,3-ring closure (dioxirane route), which yields probably the vibrationally excited oxobutanoic acid, $[C_2H_5C(O)C(O)OH]^*$, irrespective of the *E*- or *Z*-configuration of the CI (reaction (R6a)). This implies that both the propionyl peroxy radical and the subsequent reaction products as well as propionic acid, not accounted for by RO_2 reactions, arise from the decomposition of $[C_2H_5C(O)C(O)OH]^*$. Alternatively, the carbonyl-substituted CI might isomerize into vibrationally excited formic propionic anhydride, $[C_2H_5C(O)OC(O)H]^*$:

$$[C_2H_5C(O)CHOO]^* \rightarrow [C_2H_5C(O)C(O)OH]^* \quad (R6a)$$

$$[C_2H_5C(O)CHOO]^* \rightarrow [C_2H_5C(O)OC(O)H]^* \quad (R6b)$$

One should note that at least some of the reaction products could also result from the decomposition of the excited anhydride. However, it is unclear to which extent the migration of a $C_2H_5C(O)$ group competes with the migration of an H atom in the intermediately formed bis(oxy) biradical. Therefore, since a direct detection of the excited intermediates (both acid and anhydride) is not possible, we postulate the reaction products to arise from the decomposition of the oxoacid.

Fragmentation routes of vibrationally excited acids were reported only for $[HC(O)OH]^*$ and $[CH_3C(O)OH]^*$, although the data level remains relatively scarce[14] and no such data are available for substituted acids. Based on the observed reaction products, we propose here 7 possible distinct fragmentation routes for the vibrationally excited oxobutanoic acid. Accordingly, 4 fragmentation pathways are following a bond cleavage, which, in turn, result in the formation of the radical species confirmed by the observed products. The bond scission may occur either between the H and O atom of the OH group or between the OH and the carbonyl group. The remaining radical will readily eliminate either CO_2 or CO. However, in both cases, a propionyl radical is formed, which, in the presence of O_2, is immediately converted into a propionyl peroxy radical.

$$[C_2H_5C(O)C(O)OH]^* \rightarrow C_2H_5C(O) + CO_2 + H \quad (R7a)$$

$$[C_2H_5C(O)C(O)OH]^* \rightarrow C_2H_5C(O) + CO + OH \quad (R7b)$$

Theoretically, fragmentation might also occur by scission of the bond between both carbonyl groups yielding, in the presence of O_2, the same products as reaction (R7a), namely propionyl peroxy + CO_2 + HO_2.

$$[C_2H_5C(O)C(O)OH]^* \rightarrow C_2H_5C(O) + C(O)OH \quad (R7c)$$

Another radical-forming channel is conceivable, where the bond cleavage occurs between the alkyl and the carbonyl group:

$$[C_2H_5C(O)C(O)OH]^* \rightarrow C_2H_5 + CO + C(O)OH \quad (R7d)$$

Thereupon, an ethyl peroxy radical, HO_2, CO and CO_2 should be ultimately formed in the presence of O_2.

As discussed above, it is presently not clear, if ethyl peroxy radicals are formed promptly from the EVK + O_3 reaction or result only from the propionyl peroxy radical further chemistry. Regardless of the relative branching ratios for the above-mentioned decomposition channels, the formation of propionyl peroxy radicals would dominate, as concluded from the experimental results.

Since an additional source of propionic acid is necessarily related also to the chemically activated carbonyl-substituted CI, propionic acid appears to arise from a molecular fragmentation pathway.

$$[C_2H_5C(O)C(O)OH]^* \rightarrow C_2H_5C(O)OH + CO \quad (R7e)$$

Although a direct comparison is not given, at least the fact that the fragmentation yields stable molecules is in agreement with previous observations made for $[HC(O)OH]^*$ and $[CH_3C(O)OH]^*$ (see ref. 14 and references therein).

Another possible molecular fragmentation route were the elimination of CO_2 and the consecutive formation of propionaldehyde.

$$[C_2H_5C(O)C(O)OH]^* \rightarrow C_2H_5C(O)H + CO_2 \quad (R7f)$$

However, the identification of propionaldehyde is not conclusively confirmed. Although small absorption observed in the range of 2750–2680 cm^{-1} of the residual FTIR spectra might indicate its formation, the intensity is too low to permit a reliable assignment to the C_3-aldehyde. The evolution of the *m*/*z* 59 signal is as well not an unambiguous proof for propionaldehyde being more likely a fragment ion of 2-oxobutanal.

A molecular fragmentation route similar to the ketene formation as observed in the case of the vibrationally excited acetic acid might also occur. Accordingly, one would expect the formation of methyl ketene and HC(O)OH.

$$[C_2H_5C(O)C(O)OH]^* \rightarrow CH_3CH{=}C{=}O + HC(O)OH \quad (R7g)$$

Since $C_2H_5C(O)^+$ ions interfere at m/z 57, an increase of the ion signal is not necessarily a reliable proof for methyl ketene formation.

In principle, the formation of formic acid is also possible from the $CH_2OO + SO_2$ reaction. Hatakeyama *et al.*[41] suggested this reaction to proceed initially *via* the reversible formation of an adduct, which decomposes into HC(O)OH and SO_2. It was further shown that higher SO_2 levels lower the HC(O)OH yield. Theoretical calculations indicate that the further fate of the initially formed adduct evolves mainly into $HCHO + SO_3$, whereas only 17% result into the formation of a singlet bis(oxy) biradical.[26] This, in turn, might isomerize and yield at least partly stabilized formic acid. Accordingly, a contribution of $CH_2OO + SO_2$ to the overall HC(O)OH yield is actually possible. However, since there is strong evidence for formic acid formation in the absence of SO_2 (formic acid and FA), this cannot be the major source of formic acid.

Aside from that, the chemically activated fraction of CH_2OO is expected to isomerize into vibrationally excited formic acid, [HC(O)OH]*, for which decomposition was reported exclusively.[14] The only closed-shell reaction products are CO and CO_2.[14] The latter one therefore contributes to the CO_2 yield observed. However, due to the unexpectedly high HC(O)OH yield found here, it appears possible that [HC(O)OH]* is partly stabilized. This may be interpreted in terms of a low vibrational excitation that allows a competition between decomposition and collisional stabilization.

Overall, the HC(O)OH observed in both experimental set-ups (FA and HC(O)OH in the absence of SO_2, HC(O)OH in the presence of SO_2) proves its formation from chemically activated CIs. However, it does not prove unequivocally any of the above discussed formation routes. The overall ozonolysis mechanism suggested for EVK based on our findings is presented in Fig. 7.

Conclusions

The present work revealed that the ozonolysis reaction of EVK in the gas-phase is a source of formic and propionic acid with an overall carboxylic acid yield of about 29 ± 7% under these experimental conditions. Bimolecular reactions of the propionyl peroxy radical did contribute to the formation of propionic acid. However, our analysis revealed that >50% of the propionic acid observed is not accounted for by RO_2 reactions. We proposed three different pathways, as summarized in Fig. 8 explaining the formation of both formic and propionic acid.

The SO_2 consumption indicated that about 40 ± 9% of the CIs formed in the EVK + O_3 reaction are stabilized and hence prone to bimolecular reactions, particularly with H_2O and $(H_2O)_2$ under tropospheric conditions. Irrespective of the pathway yielding

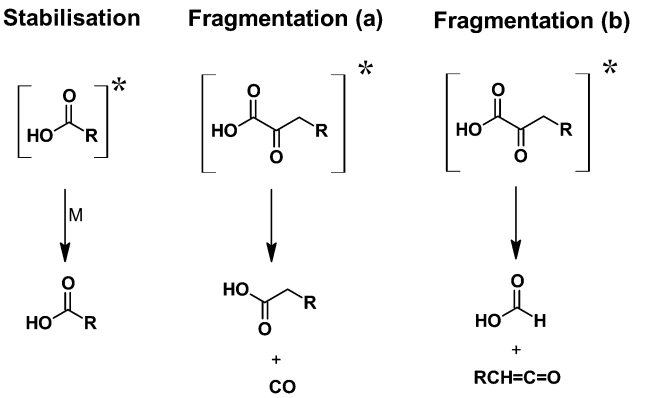

Fig. 8 Acid-forming pathways proposed within this work from chemically activated acids.

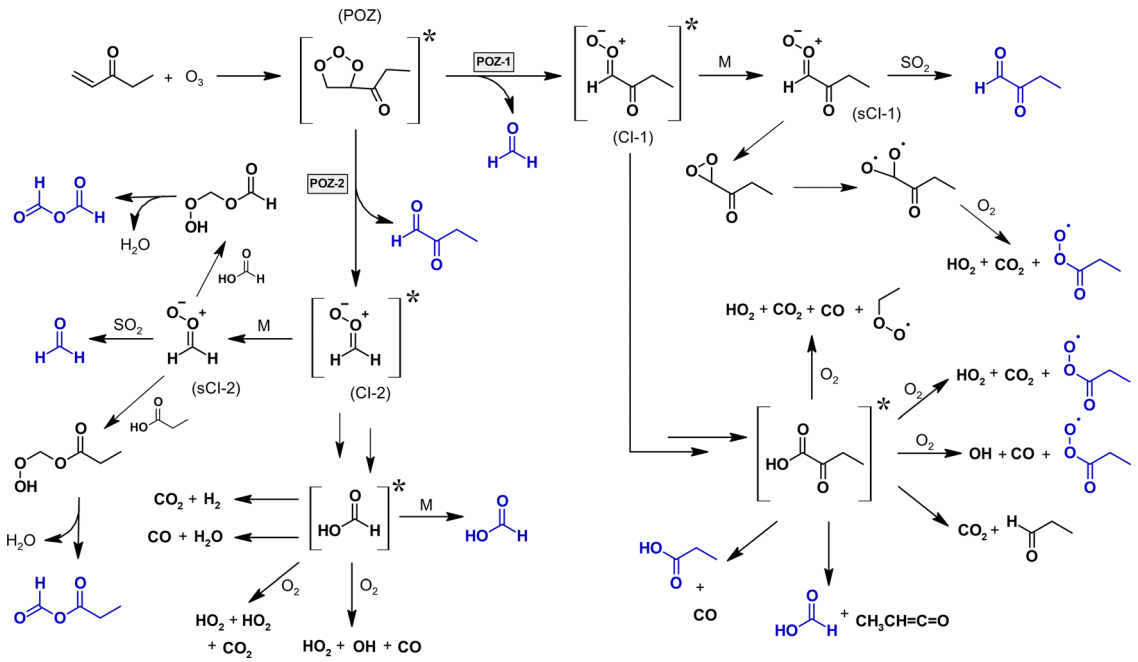

Fig. 7 Mechanism of the EVK + O_3 reaction built on the results of the present investigation. The structures are marked in blue for species quantified within this work and for radical species, whose presence is indirectly proven by the quantification of subsequently formed species. For clarity, only the *E*-isomer is drawn for the carbonyl-substituted CI. The pathways of (CI-1) are developed in detail in the text.

HC(O)OH, the present study provides strong evidence that both acids are formed from chemically activated CIs. Accordingly, both formic and propionic acid should also be formed under the humid conditions present in the troposphere.

The impact on the acid budget might be limited in the case of EVK. However, this will change dramatically if the same mechanism applies to MVK ozonolysis (accordingly yielding formic and acetic acid). Under low-NO conditions, the OH-initiated oxidation of isoprene results in about 50% MVK.[42] As stated in the introduction, under typical daytime conditions about 17% of MVK is consumed *via* the ozonolysis reaction. Considering the yearly emission strength of isoprene[43] and assuming a similar overall carboxylic acid yield from MVK + O_3, the acid production might be as high as about 4 Tg a^{-1} for HC(O)OH and 7 Tg a^{-1} for acetic acid. Clearly, there is an urgent need for better characterization of the MVK ozonolysis reaction, which will be covered in follow-up work.[44]

Conflicts of interest

There are no conflicts to declare.

Acknowledgements

The authors gratefully acknowledge funding from the Deutsche Forschungsgemeinschaft (DFG) through the grant agreement WI 958/18-1.

References

1 A. Chebbi and P. Carlier, Carboxylic acids in the troposphere, occurrence, sources, and sinks: A review, *Atmos. Environ.*, 1996, **30**, 4233–4249.
2 P. Khare, N. Kumar, K. M. Kumari and S. S. Srivastava, Atmospheric formic and acetic acids: an overiew, *Rev. Geophys.*, 1999, **37**, 227–248.
3 S. Yu, Role of organic acids (formic, acetic, pyruvic and oxalic) in the formation of cloud condensation nuclei (CCN): a review, *Atmos. Res.*, 2000, **53**, 185–217.
4 F. Paulot, D. Wunch, J. D. Crounse, G. C. Toon, D. B. Millet, P. F. DeCarlo, C. Vigouroux, N. M. Deutscher, G. González Abad, J. Notholt, T. Warneke, J. W. Hannigan, C. Warneke, J. A. de Gouw, E. J. Dunlea, M. De Mazière, D. W. T. Griffith, P. Bernath, J. L. Jimenez and P. O. Wennberg, Importance of secondary sources in the atmospheric budgets of formic and acetic acids, *Atmos. Chem. Phys.*, 2011, **11**, 1989–2013.
5 D. B. Millet, M. Baasandorj, D. K. Farmer, J. A. Thornton, K. Baumann, P. Brophy, S. Chaliyakunnel, J. A. de Gouw, M. Graus, L. Hu, A. Koss, B. H. Lee, F. D. Lopez-Hilfiker, J. A. Neuman, F. Paulot, J. Peischl, I. B. Pollack, T. B. Ryerson, C. Warneke, B. J. Williams and J. Xu, A large and ubiquitous source of atmospheric formic acid, *Atmos. Chem. Phys.*, 2015, **15**, 6283–6304.
6 S. Chaliyakunnel, D. B. Millet, K. C. Wells, K. E. Cady-Pereira and M. W. Shephard, A Large Underestimate of Formic Acid from Tropical Fires: Constraints from Space-Borne Measurements, *Environ. Sci. Technol.*, 2016, **50**, 5631–5640.
7 F. Paulot, J. D. Crounse, H. G. Kjaergaard, J. H. Kroll, J. H. Seinfeld and P. O. Wennberg, Isoprene photooxidation: new insights into the production of acids and organic nitrates, *Atmos. Chem. Phys.*, 2009, **9**, 1479–1501.
8 N. I. Butkovskaya, N. Pouvesle, A. Kukui and G. Le Bras, Mechanism of the OH-Initiated Oxidation of Glycolaldehyde over the Temperature Range 233–296 K, *J. Phys. Chem. A*, 2006, **110**, 13492–13499.
9 N. I. Butkovskaya, N. Pouvesle, A. Kukui, Y. Mu and G. Le Bras, Mechanism of the OH-Initiated Oxidation of Hydroxyacetone over the Temperature Range 236–298 K, *J. Phys. Chem. A*, 2006, **110**, 6833–6843.
10 S. So, U. Wille and G. da Silva, Atmospheric Chemistry of Enols: A Theoretical Study of the Vinyl Alcohol + OH + O_2 Reaction Mechanism, *Environ. Sci. Technol.*, 2014, **48**, 6694–6701.
11 J. S. Francisco and W. Eisfeld, Atmospheric oxidation mechanism of hydroxymethyl hydroperoxide, *J. Phys. Chem. A*, 2009, **113**, 7593–7600.
12 T. B. Nguyen, G. S. Tyndall, J. D. Crounse, A. P. Teng, K. H. Bates, R. H. Schwantes, M. M. Coggon, L. Zhang, P. Feiner, D. O. Miller, K. M. Skog, J. C. Rivera-Rios, M. Dorris, K. F. Olson, A. Koss, R. J. Wild, S. S. Brown, A. H. Goldstein, J. A. de Gouw, W. H. Brune, F. N. Keutsch, J. H. Seinfeld and P. O. Wennberg, Atmospheric fates of Criegee intermediates in the ozonolysis of isoprene, *Phys. Chem. Chem. Phys.*, 2016, **18**, 10241–10254.
13 S. Wang, M. J. Newland, W. Deng, A. R. Rickard, J. F. Hamilton, A. Muñoz, M. Ródenas, M. M. Vázquez, L. Wang and X. Wang, Aromatic Photo-oxidation, A New Source of Atmospheric Acidity, *Environ. Sci. Technol.*, 2020, **54**, 7798–7806.
14 R. A. Cox, M. Ammann, J. N. Crowley, H. Herrmann, M. E. Jenkin, V. F. McNeill, A. Mellouki, J. Troe and T. J. Wallington, Evaluated kinetic and photochemical data for atmospheric chemistry: Volume VII – Criegee intermediates, *Atmos. Chem. Phys.*, 2020, **20**, 13497–13519.
15 R. Fall, T. Karl, A. Jordan and W. Lindinger, Biogenic C5 VOCs: release from leaves after freeze-thaw wounding and occurrence in air at high mountain observatory, *Atmos. Environ.*, 2001, **35**, 3905–3916.
16 E. Grosjean, D. Grosjean and J. H. Seinfeld, Gas-Phase Reaction of Ozone with Trans-2-Hexenal, Trans-2-Hexenyl Acetate, Ethylvinyl Ketone, and 6-Methyl-5-Hepten-2-One, *Int. J. Chem. Kinet.*, 1996, **28**, 373–382.
17 Y. Ren, B. Grosselin, V. Daële and A. Mellouki, Investigation of the reaction of ozone with isoprene, methacrolein and methyl vinyl ketone using the HELIOS chamber, *Faraday Discuss.*, 2017, **200**, 289–311.
18 M. A. O'Dwyer, T. J. Carey, R. M. Healy, J. C. Wenger, B. Picquet-Varrault and J. F. Doussin, The Gas-phase Ozonolysis of 1-Penten-3-ol, (Z)-2-Penten-1-ol and 1-Penten-3-one: Kinetics, Products and Secondary Organic Aerosol Formation, *Z. Phys. Chem.*, 2010, **224**, 1059–1080.
19 A. Mellouki, M. Ammann, R. A. Cox, J. N. Crowley, H. Herrmann, M. E. Jenkin, V. F. McNeill, J. Troe and

T. J. Wallington, Evaluated kinetic and photochemical data for atmospheric chemistry: volume VIII – gas-phase reactions of organic species with four, or more, carbon atoms ($\geq$ C4), *Atmos. Chem. Phys.*, 2021, **21**, 4797–4808.

20 J. N. Illmann, I. Patroescu-Klotz and P. Wiesen, Gas-phase reactivity of acyclic α,β-unsaturated carbonyls towards ozone, *Phys. Chem. Chem. Phys.*, 2021, **23**, 3455–3466.

21 M. B. Blanco and M. A. Teruel, Atmospheric photodegradation of ethyl vinyl ketone and vinyl propionate initiated by OH radicals, *Chem. Phys. Lett.*, 2011, **502**, 159–162.

22 D. Grosjean, E. Grosjean and E. L. Williams, II, Rate constants for the gas-phase reactions of ozone with unsaturated alcohols, esters, and carbonyls, *Int. J. Chem. Kinet.*, 1993, **25**, 783–794.

23 N. Illmann, R. G. Gibilisco, I. G. Bejan, I. Patroescu-Klotz and P. Wiesen, Atmospheric oxidation of α,β-unsaturated ketones: kinetics and mechanism of the OH radical reaction, *Atmos. Chem. Phys.*, 2021, **21**, 13667–13686.

24 N. Illmann, I. Patroescu-Klotz and P. Wiesen, Biomass burning plume chemistry: OH-radical-initiated oxidation of 3-penten-2-one and its main oxidation product 2-hydroxypropanal, *Atmos. Chem. Phys.*, 2021, **21**, 18557–18572.

25 R. Criegee, Mechanism of Ozonolysis, *Angew. Chem.*, 1975, **14**, 745–752.

26 L. Vereecken, H. Harder and A. Novelli, The reaction of Criegee intermediates with NO, RO_2, and SO_2, and their fate in the atmosphere, *Phys. Chem. Chem. Phys.*, 2012, **14**, 14682–14695.

27 L. Vereecken, A. Novelli and D. Taraborrelli, Unimolecular decay strongly limits the atmospheric impact of Criegee intermediates, *Phys. Chem. Chem. Phys.*, 2017, **19**, 31599–31612.

28 R. K. Talukdar, L. Zhu, K. J. Feierabend and J. B. Burkholder, Rate coefficients for the reaction of methylglyoxal (CH_3CO-CHO) with OH and NO_3 and glyoxal $(HCO)_2$ with NO_3, *Atmos. Chem. Phys.*, 2011, **11**, 10837–10851.

29 J. J. Orlando, G. S. Tyndall, L. Vereecken and J. Peeters, The Atmospheric Chemistry of the Acetonoxy Radical, *J. Phys. Chem. A*, 2000, **104**, 11578–11588.

30 P. Neeb, O. Horie and G. K. Moortgat, The nature of the transitory product in the gas-phase ozonolysis of ethene, *Chem. Phys. Lett.*, 1995, **246**, 150–156.

31 P. Neeb, O. Horie and G. K. Moortgat, Gas-Phase Ozonolysis of Ethene in the Presence of Hydroxylic Compounds, *Int. J. Chem. Kinet.*, 1996, **28**, 721–730.

32 P. Neeb, F. Sauer, O. Horie and G. K. Moortgat, Formation of hydroxymethyl hydroperoxide and formic acid in alkene ozonolysis in the presence of water vapour, *Atmos. Environ.*, 1997, **31**, 1417–1423.

33 L. Sheps, B. Rotavera, A. J. Eskola, D. L. Osborn, C. A. Taatjes, K. Au, D. E. Shallcross, M. A. H. Khan and C. J. Percival, The reaction of Criegee intermediate CH_2OO with water dimer: primary products and atmospheric impact, *Phys. Chem. Chem. Phys.*, 2017, **19**, 21970–21979.

34 A. S. Hasson, G. S. Tyndall and J. J. Orlando, A Product Yield Study of the Reaction of HO_2 Radicals with Ethyl Peroxy ($C_2H_5O_2$), Acetyl Peroxy ($CH_3C(O)O_2$), and Acetonyl Peroxy ($CH_3C(O)CH2O2$) Radicals, *J. Phys. Chem. A*, 2004, **108**, 5979–5989.

35 J.-P. Le Crâne, E. Villenave, M. D. Hurley, T. J. Wallington and J. C. Ball, Atmospheric Chemistry of Propionaldehyde: Kinetics and Mechanisms of Reactions with OH Radicals and Cl Atoms, UV Spectrum, and Self-Reaction Kinetics of $CH_3CH_2C(O)O_2$ Radicals at 298 K, *J. Phys. Chem. A*, 2005, **109**, 11837–11850.

36 A. C. Noell, L. S. Alconcel, D. J. Robichaud, M. Okumura and S. P. Sander, Near-Infrared Kinetic Spectroscopy of the HO_2 and $C_2H_5O_2$ Self-reactions and Cross-Reactions, *J. Phys. Chem. A*, 2010, **114**, 6983–6995.

37 A. S. Hasson, G. S. Tyndall, J. J. Orlando, S. Singh, S. Q. Hernandez, S. Campbell and Y. Ibarra, Branching Ratios for the Reaction of Selected Carbonyl-Containing Peroxy Radicals with Hydroperoxy Radicals, *J. Phys. Chem. A*, 2012, **116**, 6264–6281.

38 T. L. Nguyen, R. Winterhalter, G. Moortgat, B. Kanawati, J. Peeters and L. Vereecken, The gas-phase ozonolysis of β-caryophyllene ($C_{15}H_{24}$). Part II: A theoretical study, *Phys. Chem. Chem. Phys.*, 2009, **11**, 4173–4183.

39 T. L. Nguyen, J. Peeters and L. Vereecken, Theoretical study of the gas-phase ozonolysis of β-pinene ($C_{10}H_{16}$), *Phys. Chem. Chem. Phys.*, 2009, **11**, 5643–5656.

40 R. Winterhalter, F. Herrmann, B. Kanawati, T. L. Nguyen, J. Peeters, L. Vereecken and G. K. Moortgat, The gas-phase ozonolysis of of β-caryophyllene ($C_{15}H_{24}$). Part I: an experimental study, *Phys. Chem. Chem. Phys.*, 2009, **11**, 4152–4172.

41 S. Hatakeyama, H. Kobayashi, Z.-Y. Lin, H. Takagi and H. Akimoto, Mechanism for the Reaction of CH_2OO with SO_2, *J. Phys. Chem.*, 1986, **90**, 4131–4135.

42 M. E. Jenkin, J. C. Young and A. R. Rickard, The MCM v3.3.1 degradation scheme for isoprene, *Atmos. Chem. Phys.*, 2015, **15**, 11433–11459.

43 A. Guenther, T. Karl, P. Harley, C. Wiedinmyer, P. I. Palmer and C. Geron, Estimates of global terrestrial isoprene emissions using MEGAN (Model of Emissions of Gases and Aerosols from Nature), *Atmos. Chem. Phys.*, 2006, **6**, 3181–3210.

44 N. Illmann, I. Patroescu-Klotz and P. Wiesen, Methyl vinyl ketone + O3: A Source of Carboxylic Acids in the Troposphere, manuscript in preparation.